Replication-dependent size reduction precedes differentiation in *Chlamydia trachomatis*

Jennifer K. Lee[1‡], Germán A. Enciso[2‡], Daniela Boassa[4], Christopher N. Chander[1], Tracy H. Lou[1], Sean S. Pairawan[1], Melody C. Guo[1], Fred Wan[2], Mark H. Ellisman[4,5,6], Christine Sütterlin[1*] and Ming Tan[3]

[1] Department of Developmental and Cell Biology, [2] Department of Mathematics, [3] Departments of Microbiology & Molecular Genetics, and Medicine, University of California, Irvine, CA, 92697-2300, USA

[4] National Center for Microscopy and Imaging Research and Center for Research on Biological Systems, [5] Department of Neurosciences University of California, San Diego, La Jolla, CA 92093, USA

[6] Salk Institute for Biological Studies, San Diego, CA 92037, USA

‡These authors contributed equally to this work

*Corresponding author: Christine Sütterlin, email: suetterc@uci.edu, Tel: (949) 824-7140

Key words: *Chlamydia*, intracellular infection, developmental cycle, replication, differentiation, asynchrony, cell size control, serial block-face scanning electron microscopy, mathematical modeling

Chlamydia trachomatis is the most common cause of bacterial sexually transmitted infection [1,2] and accounts for 60% of infectious disease cases reported in the U.S. [3]. It also causes trachoma, a communicable blindness that affects 40 million people in underdeveloped countries [4]. The unusual intracellular *Chlamydia* infection is marked by conversion between two developmental forms of the bacterium inside a eukaryotic host cell [5]. A vegetative form called the reticulate body (RB) divides repeatedly and then converts into an elementary body (EB), which is an environmentally stable infectious form, for transmission to a new host cell. The signal for this cell fate decision is unknown. Here we used a quantitative three-dimensional electron microscopy approach to provide evidence that RBs divide by binary fission and to measure an unprecedented six-fold reduction in average RB size as the RB population expanded. Conversion only occurred after at least six rounds of RB replication and correlated with smaller RB size. These results suggest that RBs only convert into EBs below a size threshold, which they reach by repeatedly dividing before doubling in size. To understand the implications of these findings, we generated a stochastic mathematical model, which showed how replication-dependent RB size reduction produces delayed and asynchronous conversion, which are hallmarks of the *Chlamydia* developmental cycle. Our findings are consistent with a novel size control model in which an external signal is not necessary to control the timing of RB-to-EB conversion.

A biphasic developmental cycle is a defining feature of *C. trachomatis* and other obligate intracellular bacteria that belong to the genus *Chlamydia* [5,6]. It begins when the EB enters an epithelial cell where it converts into the larger, metabolically-active RB

within a membrane-bound compartment called the chlamydial inclusion. Beginning at 9-12 hours post infection (hpi), RBs divide repeatedly to produce several hundred to a thousand progeny. However, RBs are not infectious and must differentiate into an EB for transmission of the infection to a new host cell. RB-to-EB conversion is first detected at about 24 hpi but occurs asynchronously. This unusual developmental cycle ends at 40-48 hpi with release of EBs to infect new host cells.

The serial conversion between two specialized chlamydial forms raises questions about how these developmental events are regulated. The RB can either divide into two daughter RBs or convert into an ER, making it the stem cell for RB production and the progenitor of the infectious EB. The signal and control mechanism for this cell fate decision are not known. Although the EB is functionally analogous to a spore, it is produced from an RB by cellular differentiation and not by asymmetric cell division of a vegetative bacterial cell as is the case for the *Bacillus* spore [7].

There has been no quantitative analysis of the dynamics of RB-to-EB conversion. The major limitation has been the size of the chlamydial inclusion, which eventually occupies most of the cytoplasm. Conventional two-dimensional (2D) electron micrographs have provided a sampling of the inclusion and have shown that RB-to-EB conversion occurs in a delayed and asynchronous manner [8,9]. However, the numbers and relative proportions of RBs and EBs have not been determined over the course of the developmental cycle. Upon re-examination, these electron micrographs reveal that the first few RBs in an inclusion are generally larger than the RB population at later times, although this difference has not been remarked upon.

Serial block-face scanning EM (SBEM) is a relative novel volume EM technique [10,11] to study the structure of biological objects. It has been commonly applied in neuroscience for 3D visualization of the nervous system ultrastructure [12,13] and for circuit reconstructions [10,11,14,15]. More recently it has been used with cell culture models to investigate the 3D architecture of organelles, subcellular structures, DNA and viral proteins [16-18]. However, this powerful method has not been used to investigate an infection with a pathogenic bacterium.

In this study, we used SBEM to provide a comprehensive quantitative analysis of the chlamydial infection over time. We show that RBs divide by binary fission and that RB size is heterogeneous and decreases with sequential rounds of . These experimental data, together with a a size control model that asynchronous and delayed onset of RB-to-EB conversion.

We performed SBEM on monolayers of *C. trachomatis*-infected HeLa cells (Fig. S1A), which required up to 277 EM sections to analyze an entire inclusion. In each section, we identified and traced the inclusion membrane and four chlamydial forms (Fig. S1B). We readily distinguished RBs from smaller, electron-dense EBs, and separately counted dividing RBs, which are replication intermediates with a constriction that produces a characteristic dumb-bell shape. We also identified a conversion intermediate called the intermediate body (IB), which has a target-like appearance from DNA condensation beginning in its center [5]. Each EM section had a thickness of 0.06 μm, which allowed individual bacteria to be observed and seqmented in multiple successive sections, increasing the accuracy of identification and physical measurements. On

average, each EB was analyzed with 6-7 consecutive EM sections and each RB was analyzed with 11-21 EM sections. We then combined all the EM sections computationally into a 3D reconstruction of the inclusion (Fig. 1A and Movie S1).

Our analysis provided unprecedented detailed quantitative information about the *C. trachomatis* inclusion and its developmental forms, but was time and labor intensive. For example, the image acquisition time for each EM section was 3 minutes, but a monolayer of infected cells required up to 500 sections and took a total of 25 hours. The outline of each bacterium in every EM section was individually traced in a process called segmentation. Segmentation of EBs was semi-automated because of their uniform size and circular shape. However RBs required manual segmentation because they varied in size and had an irregular shape. Early inclusions containing few chlamydiae within a small number of EM sections were easily analyzed, but inclusions from late in the developmental cycle each required several days to segment because they contained about a thousand RBs, dividing RBs, IBs and EBs.

Our 3D EM analysis revealed a non-uniform distribution of chlamydial developmental forms in the inclusion. The proportions of the four forms differed between the entire inclusion and single sections (Fig. 1A and S1C). In particular, sections near the pole of the inclusion overrepresented the percentage of dividing RBs (section 154 in Fig. S1C). These findings illustrate the sampling bias inherent to conventional 2D EM analysis, which only examines a small part of the inclusion. In contrast, our 3D EM approach allows a comprehensive, quantitative analysis of the large and heterogeneous chlamydial inclusion.

To measure dynamic changes in the numbers, proportions and sizes of chlamydial developmental forms, we analyzed infected cells over the time course of the intracellular infection (Fig. 1B). For validation, our quantifications compared well with conventional methods for measuring average number of chlamydial genomes/cell by qPCR (Fig. S2A) and infectious EBs with a progeny assay (Fig. S2B). From counting all chlamydiae in the inclusions analyzed, we calculated a chlamydial doubling time of 1.8 hours between 12 and 24 hpi, which is similar to published studies [8]. We measured an exponential increase in the mean number of chlamydiae per inclusion from 1.3 at 12 hpi to 1,163 at 32 hpi (Fig. 1B). Average RB number increased to a peak of 263 at 32 hpi. There were equal proportions of RBs and dividing RBs for all time points up to 32 hpi, indicating that RB replication was ongoing and that each RB spent about half of its lifespan undergoing cytokinesis. IBs, as a marker of RB-to-EB conversion, were first detected at 24 hpi, when there were an average of 105 RBs and dividing RBs. This temporal pattern indicates that at least six rounds of replication had occurred prior to the onset of conversion. At most 23% of chlamydiae were IBs at any time point, emphasizing the asynchronous nature of RB-to-EB conversion. Subsequently there was progressive accumulation of EBs to a maximum of 70% of all chlamydiae in the inclusion at 40 hpi. At late time points, after 32 hpi, there were proportionally fewer dividing RBs and IBs, indicating reductions in both RB replication and RB-to-EB conversion.

To investigate how conversion is controlled, we examined if parameters of the inclusion or its bacterial population correlated with conversion onset at 24 hpi. Mean inclusion volume increased by 300-fold from 2.9 μm^3 at 12 hpi to 900 μm^3 at 40 hpi, with

inclusion growth primarily occurring before 28 hpi (Fig. 2A). However, the density of the chlamydial population remained remarkably constant because the number of chlamydiae in the inclusion increased proportionally with inclusion volume at all times (Figs. 2A and B). In contrast, the total volume of chlamydiae within an inclusion did not keep pace with inclusion growth (Fig. 2C), causing a progressive decrease in the volume fraction of the inclusion taken up by chlamydiae (Fig. 2D). Thus RB-to-EB conversion does not appear to correlate with overall physical crowding in the inclusion, although local crowding effects cannot be excluded.

Unexpectedly, our 3D EM analysis revealed that RBs progressively decrease in size before differentiating into EBs. Mean RB volume decreased from 1.01 μm^3 (equivalent to a 1.25 μm diameter sphere) at 12 hpi, to 0.27 μm^3 at 28 hpi and 0.16 μm^3 (0.67 μm diameter) at 32 hpi, when conversion was actively underway (Fig. 3A). Dividing RBs showed a similar decrease in average size. The finding of concurrent RB replication and size reduction suggests that RBs divide before they double in size.

There was also heterogeneity in RB size within an inclusion. For example, in a single 24 hpi inclusion, the mean size of 40 RBs was 0.37 μm^3, but 25% were at or below 0.1 μm^3 with a coefficient of variation (CV, standard deviation/mean) of 97% (Fig. 3C, left panel). In a single 40 hpi inclusion, the mean size of 240 RBs was only 0.21 μm^3, with 45% at or below 0.1 μm and a CV of 118% (Fig. 3C, right panel). For comparison, *E. coli,* which maintains tight size control, had a size distribution in a steady state population with a CV of 30-40% [19]. This chlamydial size heterogeneity suggests that RB size at division is not tightly controlled.

The lack of size homeostasis in *C. trachomatis* distinguishes it from other bacteria, which maintain cell size through an "adder model" by adding a constant volume before dividing [20,21]. In nutrient-poor conditions, bacterial cells get smaller by up to two-fold because of lower growth rate [21-23], but the six-fold reduction in RB size during the intracellular chlamydial infection is unprecedented and occurred during exponential growth of the RB population (Fig. S2A). Intriguingly, the size ratio of RBs to dividing RBs remained constant at 1.5 from 16 to 40 hpi (Fig. 3B), even as both forms got smaller (Fig. 3A). This stable dividing ratio is reminiscent of the "timer" size control model in *Schizosaccharomyces pombe*, in which there is growth for a fixed time before cell division [24]. However, a *Chlamydia* timer would have to be set to less than the time required for RBs to double in size.

Ongoing size reduction is not sustainable, but we surmise that it may be tolerated by chlamydiae because of their unusual developmental cycle. The dramatic and rapid decrease in RB size occurs during a limited number of replication cycles within an infected host cell. Each RB lineage then ends with RB-to-EB conversion instead of being maintained indefinitely. We hypothesize that there is the opportunity to reset RB size when the EB infects a new cell and converts into the initial RB. Thus, size homeostasis may be less critical in *Chlamydia* because it converts back and forth between two developmental forms.

Chlamydia had been presumed to divide by binary fission [25], but a recent report described polarized cell division in *C. trachomatis* [26]. In that study, confocal and 2D electron microscopy images showed several examples of a smaller, nascent daughter cell budding off an RB. To examine if RBs replicate by binary fission or budding, we

used our 3D EM approach to analyze all 114 dividing RBs in two *C. trachomatis* inclusions at 24 hpi. We calculated the daughter/parent ratio, which is the proportion of the dividing RB parent occupied by each of its two nascent daughter cells [27]. The CV for the daughter/parent ratio was 11% (Fig. 4), which is only slightly larger than the CV of 4% calculated for *E. coli* [27]. These measurements indicate that RBs divide relatively symmetrically and are consistent with binary fission. We did not detect RBs or dividing RBs with a bud with our 3D imaging method, which should be superior to 2D EM for this task.

We also performed a statistical analysis called the D'Agostino-Pearson test [28] to determine whether polarized cell division is likely in RBs. This approach was used in a classic paper from the 1960s to show that *E. coli* divides by binary fission [27]. If cell division is mediated by binary fission, the distribution of daughter/parent ratios (Fig. 4) approximates a Gaussian curve. Conversely, polarized cell division generates a fraction of daughter cells with very small or very large daughter/parent ratios, which produces a signature graph with a fat tail, and a kurtosis, or "peakness", of the distribution that has a negative value. The distribution of daughter/parent ratios from our analysis of dividing RBs at 24 hpi had a kurtosis of 1.07, which is a positive value that indicates a strong peak and a small tail. This calculation provides quantitative evidence that chlamydiae divide by binary fission rather than by polarized cell division.

What is the significance or function of RB size reduction and size heterogeneity? While decreasing RB size may allow more chlamydiae to fit within the inclusion, there appears to be ample space within late inclusions to accommodate the bacterial population (Fig. 2C and D). Instead, the temporal association between smaller RB size

and RB-to-EB conversion suggests that there may be a permissive size for conversion. Based on this observation, we propose a size control mechanism in which RBs decrease in size through replication and only convert when they reach a minimal size threshold (Fig. 5A). According to this model, the time of conversion depends on the number of replication cycles required to become small enough to convert. If RB size decreases uniformly in a population, conversion will occur at the same time. However, if there is RB size heterogeneity, as we have detected, a variable number of replication cycles will be required to reach the conversion size, causing conversion to be asynchronous (Fig. 5A).

We designed a stochastic mathematical model to study the ramifications of this size control mechanism (Fig. 5B). We constrained this model with multiple parameters obtained from our studies (Table 1), including direct measurements (initial RB size, time of initial RB replication, variability of daughter cell size in a dividing RB), and calculated values (RB growth rate, mean transition times from small RB-to-dividing RB and from dividing RB-to-2RBs). We also used values that were fit to our data (RB growth rate variability, mean transition times from RB-to-IB and from IB-to-EB). Each RB was allowed to divide at a variable size that was on average less than twice its original size. We estimated an RB threshold size for conversion of 0.06 μm^3 from the mean size of IBs upon first appearance at 24 hpi (Fig. S3A). This putative threshold size was also the 10^{th} percentile of RB size in a 24 hpi inclusion (Fig. 3C).

This stochastic, cell-autonomous model replicates key numerical and temporal features of the chlamydial developmental cycle. It produces a progressive decrease in average RB size (Fig. 5C), and size heterogeneity within an inclusion (Fig. 5D). It also

reproduces the initial phase of RB replication without EB production, followed by delayed and asynchronous RB-to-EB conversion (Figs. 5E and F). The size control model generated growth curves that most closely resembled those of infected cells (Fig. 5G) when RBs divided at 1.6 ± 0.3 times their starting size (Mathematical Analysis in the Supplementary Materials). There has been speculation that RB-to-EB conversion is controlled by external signals, such as type III secretion and contact between the RB and the inclusion membrane [29]. However, our stochastic model demonstrates that the observed reduction in RB size could be used as a feedback-independent mechanism to control the dynamics of RB-to-EB conversion. We have not yet been able to test this stochastic model by manipulating the timing of RB replication and RB-to-EB conversion, but automation of the 3D EM segmentation step will help streamline the analysis.

How might RB size control conversion? We speculate that size reduction may facilitate conversion because a decrease in the 25-50-fold size disparity between the initial RB (average volume 1.01 μm^3, Fig. 3A) and an EB (average volume 0.02-0.04 μm^3, Fig. S3B) may make conversion more energetically favorable. Alternatively, a smaller RB could have a higher effective concentration of a conversion-promoting factor. There is also precedent for an inhibitory DNA-binding factor to be titrated out by the higher DNA-cytoplasmic ratio of a smaller cell [30]. The geometry of a smaller RB may also reduce its contact with the inclusion membrane, which has been proposed as a signal that prevents RB-to-EB conversion [29].

In summary, this study provides an unprecedented quantitative analysis of the entire chlamydial inclusion and its changing content of developmental forms over time. Our approach reveals that RBs replicate by binary fission and decrease in size with

successive rounds of replication prior to RB-to-EB conversion. This size reduction was detected even though our analysis was limited to discrete timepoints in the developmental cycle, rather than real-time measurements of bacterial size over multiple RB generations, which is not technically feasible at present. We propose that there is a minimum size threshold for RBs to convert. As a consequence, RB size may act as an intrinsic signal to delay conversion until the RB population has expanded. Our stochastic modeling shows that progressive reduction in RB size to a threshold size is sufficient to produce the delayed onset of RB-to-EB conversion without external feedback. Moreover, the asynchronous nature of conversion can be accounted for by variability in both RB size and the number of RB cell divisions to reach the threshold size. This size control model bears resemblance to midblastula transition, in which there are multiple rounds of cell division before a developmental switch during early embryogenesis [30]. Our finding of RB size reduction before differentiation suggests that *C. trachomatis* may also use its cell size as a developmental timer.

Author Contributions: J.K.L. conducted the experiments, collected, processed and analyzed 3D EM data; G.A.E. and F.W. designed, performed and analyzed mathematical modeling simulations and wrote the mathematical analysis; D.B. prepared 3D EM samples and collected and processed micrograph data; C.N.C., T.H.L., S.S.P., and M.C.G. segmented 3D EM data; C.S., M.T. and G.A.E. performed the study design and analyses; M.T. and C.S. wrote the manuscript with assistance from J.K.L. and G.A.E.

Acknowledgements: We thank A. Lander, B. Semler, E. Stanbridge and S. Gross for critical reading of the manuscript and helpful comments and A. Noske for technical help with 3D EM segmentation and analysis. This work was supported by a grant from the NIH (R21 AI117463) (M.T.) and a Research Scholar Grant from the American Cancer Society (C.S.). J.K.L. was supported by a training grant from the National Cancer Institute (T32 CA0090054). This work was also supported by a NIH grant to M.H. Ellisman (P41 GM103412) for support of the National Center for Microscopy and Imaging Research.

Figure 1. Temporal analysis of chlamydial developmental forms using a three-dimensional electron microscopy approach.

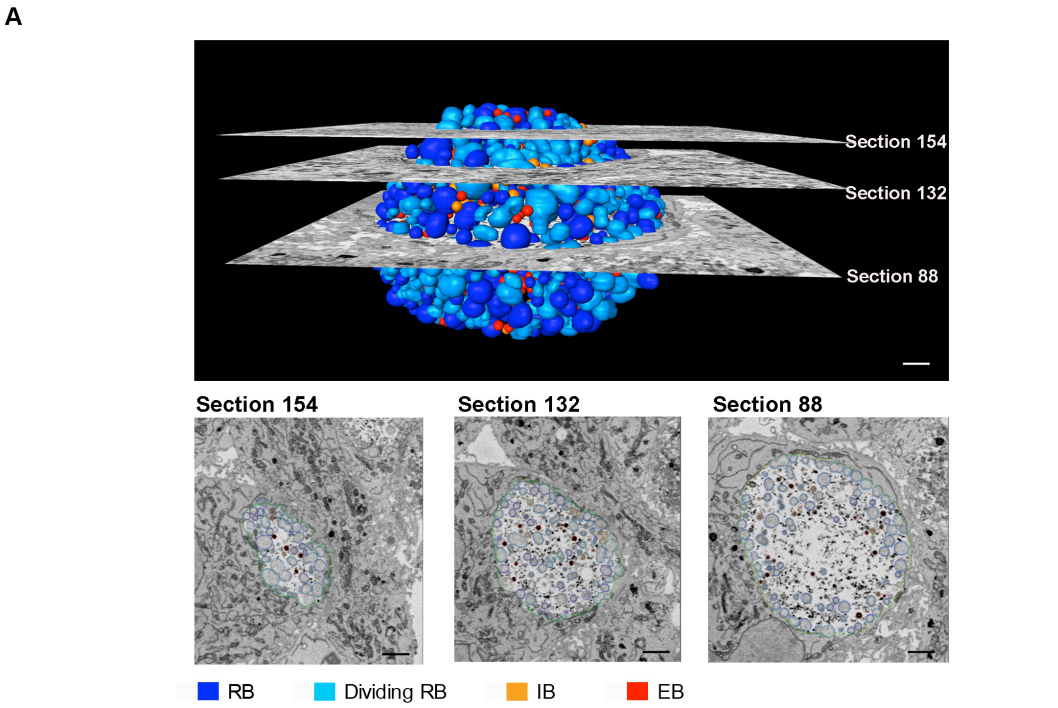

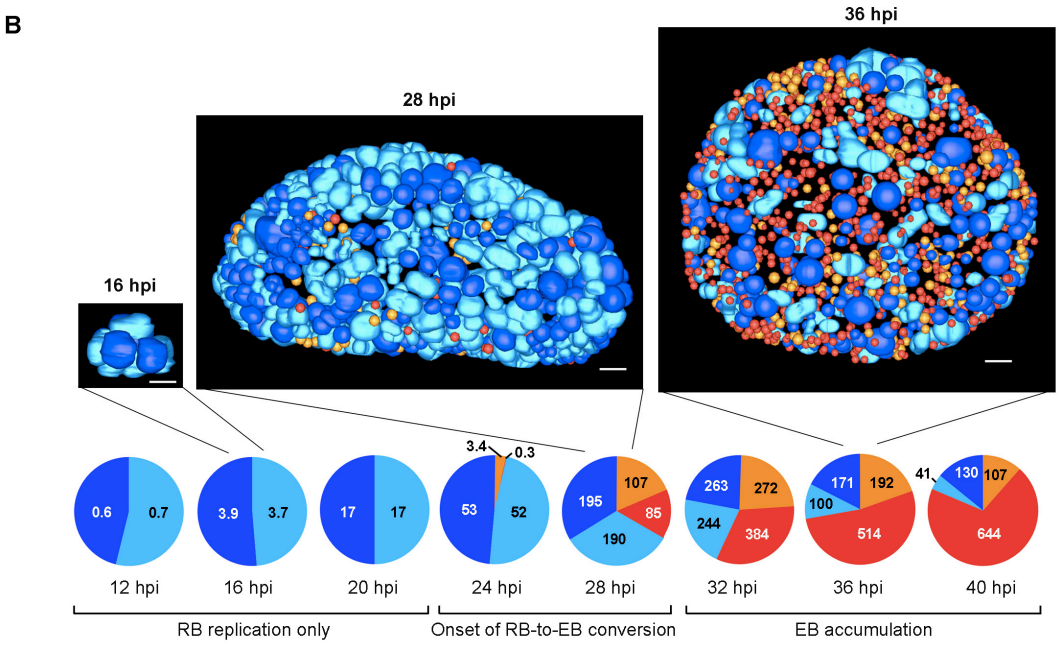

1

Figure 1. Temporal analysis of chlamydial developmental forms using a three-dimensional electron microscopy approach.

(A) Serial block-face scanning electron microscopy analysis (SBEM) was used to generate a three-dimensional computational reconstruction of the chlamydial inclusion in a *C. trachomatis*-infected HeLa cell at 28 hours post infection (hpi). Micrographs (middle) are shown for sections 154 and 132 (3/4 and halfway up from equator, respectively) and section 88 (equator), with segmentation markings for inclusion membrane (green), RBs (dark blue), dividing RBs (light blue), IBs (orange) and EBs (red). Scale bar: 1000 nm.

(B) Entire chlamydial inclusions from representative infected cells at 16, 28, and 36 hpi. Scale bar: 1000 nm. Pie charts showing mean numbers of each chlamydial form/inclusion are grouped into three developmental phases: *RB replication only* (no IBs or EBs), *Onset of RB-to-EB conversion* (IBs + EBs ≤ 50% of chlamydiae), and *EB accumulation* (IBs + EBs > 50% of chlamydiae).

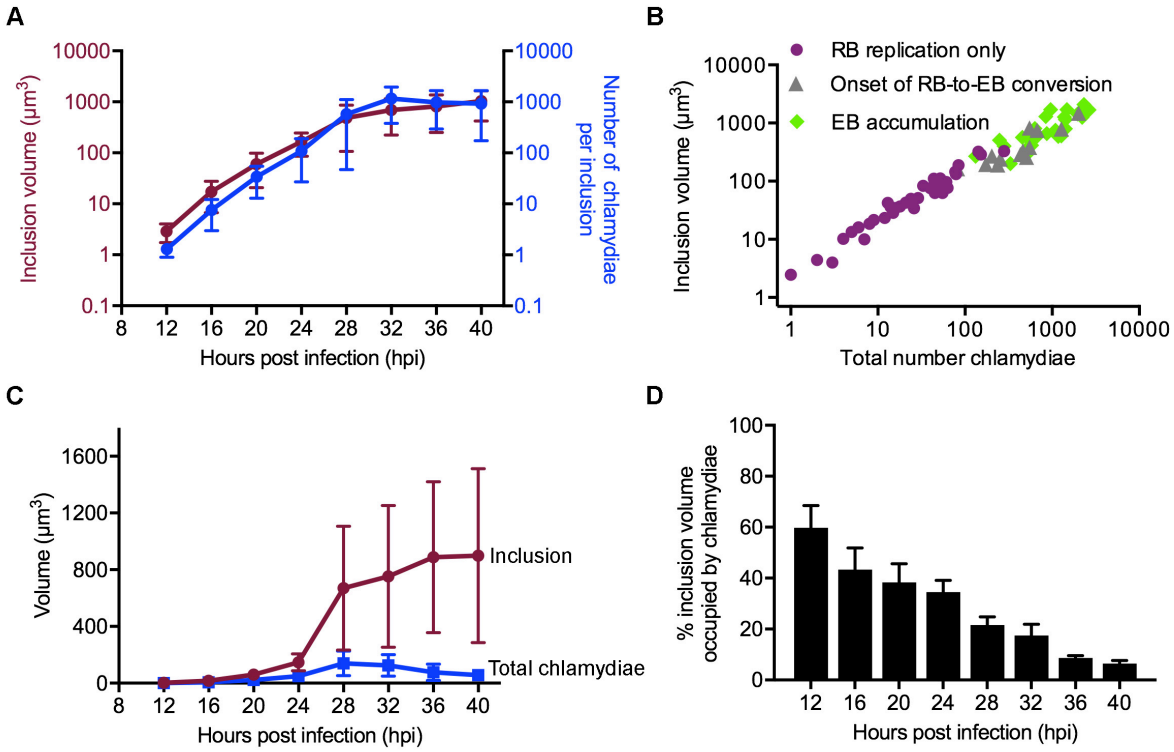

Figure 2. Volume analysis of the chlamydial inclusion and chlamydial forms during the developmental cycle.

(A) Temporal change in inclusion volume and number of chlamydiae/inclusion. Data presented in log scale. **(B)** Linear relationship between inclusion volume and total number of chlamydiae within that inclusion. Each dot represents a single inclusion, color-coded by its developmental phase, as described in Fig. 1B. **(C)** Temporal change in inclusion volume and total volume of chlamydiae within the inclusion. **(D)** % inclusion volume occupied by chlamydiae was calculated for each inclusion as total chlamydial volume divided by inclusion volume.

Figure 3. RB size decreases and becomes heterogeneous as the developmental cycle progresses.

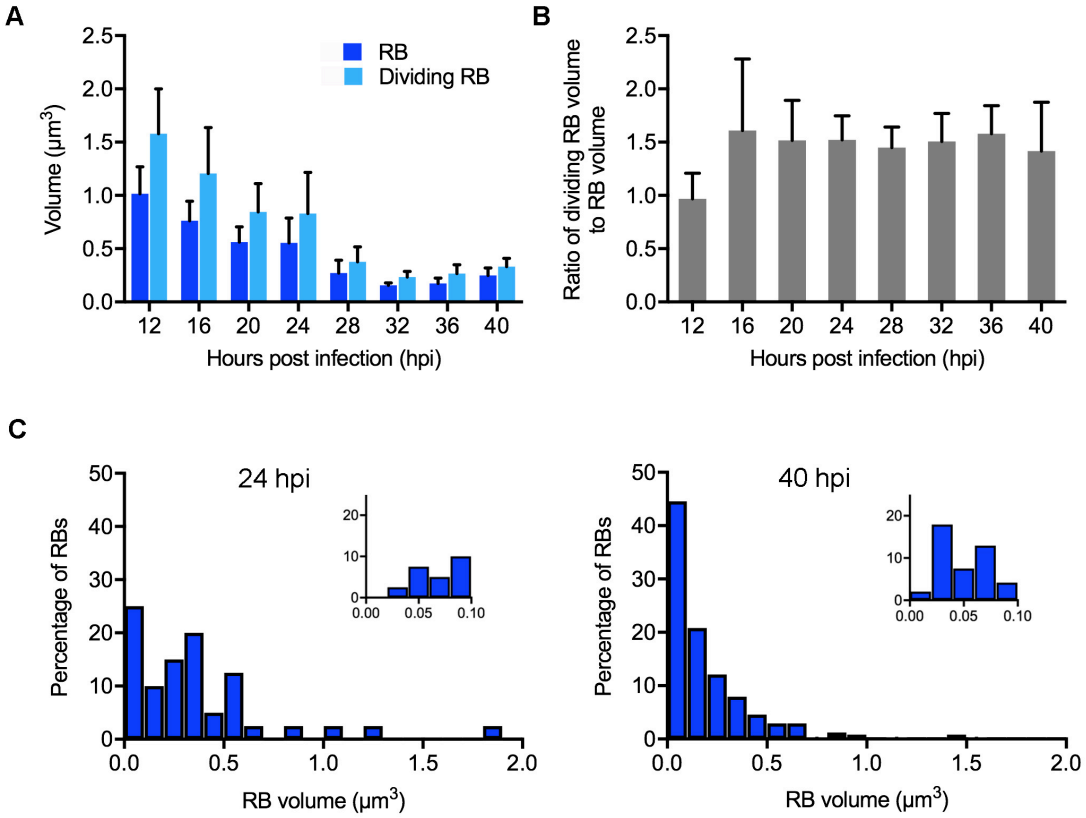

Figure 3. RB size decreases and becomes heterogeneous as the developmental cycle progresses.

(A) Temporal change in volume of RBs and dividing RBs. Average volume of all RBs or dividing RBs in each inclusion was first determined, and then reported as the mean RB or dividing RB volume for all inclusions at each time point. Mean values are reported and error bars indicate standard deviation. The decrease in RB size was statistically significant between 12 hpi and all later time points (highest p-values were between 12 and 16 hpi: $p = 0.00025$, t-value = 3.9, df = 45, and between 12 and 24 hpi: $p < 0.0001$,

t-value = 4.6, df = 28, unpaired t-test). **(B)** Ratio of dividing RB volume to RB volume during the developmental cycle. For each time point, the ratio was first determined for each inclusion, and then reported as the mean of ratios for all inclusions at that time point. **(C)** Size histograms for all RBs within a single inclusion at 24 hpi (n=40) and 40 hpi (n=240), distributed into 0.1 μm^3 bins. Insets show the smallest bin subdivided into five 0.02 μm^3 bins with same y-axis scale.

Figure 4. RB replication by binary fission.

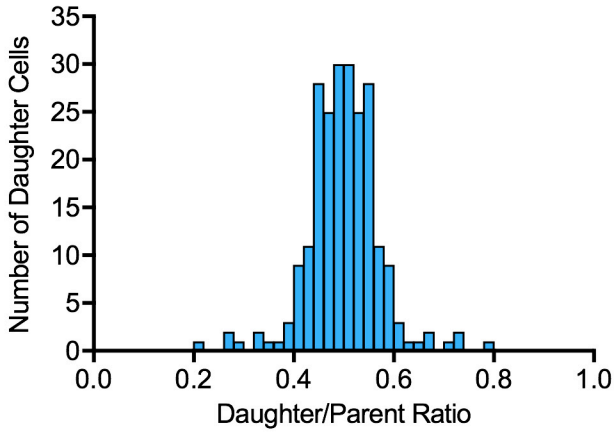

Figure 4. RB replication by binary fission.

Size histogram of nascent daughter cells at 24 hpi. The volume of each daughter cell was determined separately for 114 dividing RBs ("parent') from two 24 hpi inclusions. For each nascent daughter cell, the daughter/parent ratio was dparental dividing RB volume [27].

1

Figure 5. Analysis of size-dependent control of RB-to-EB conversion using a stochastic mathematical model.

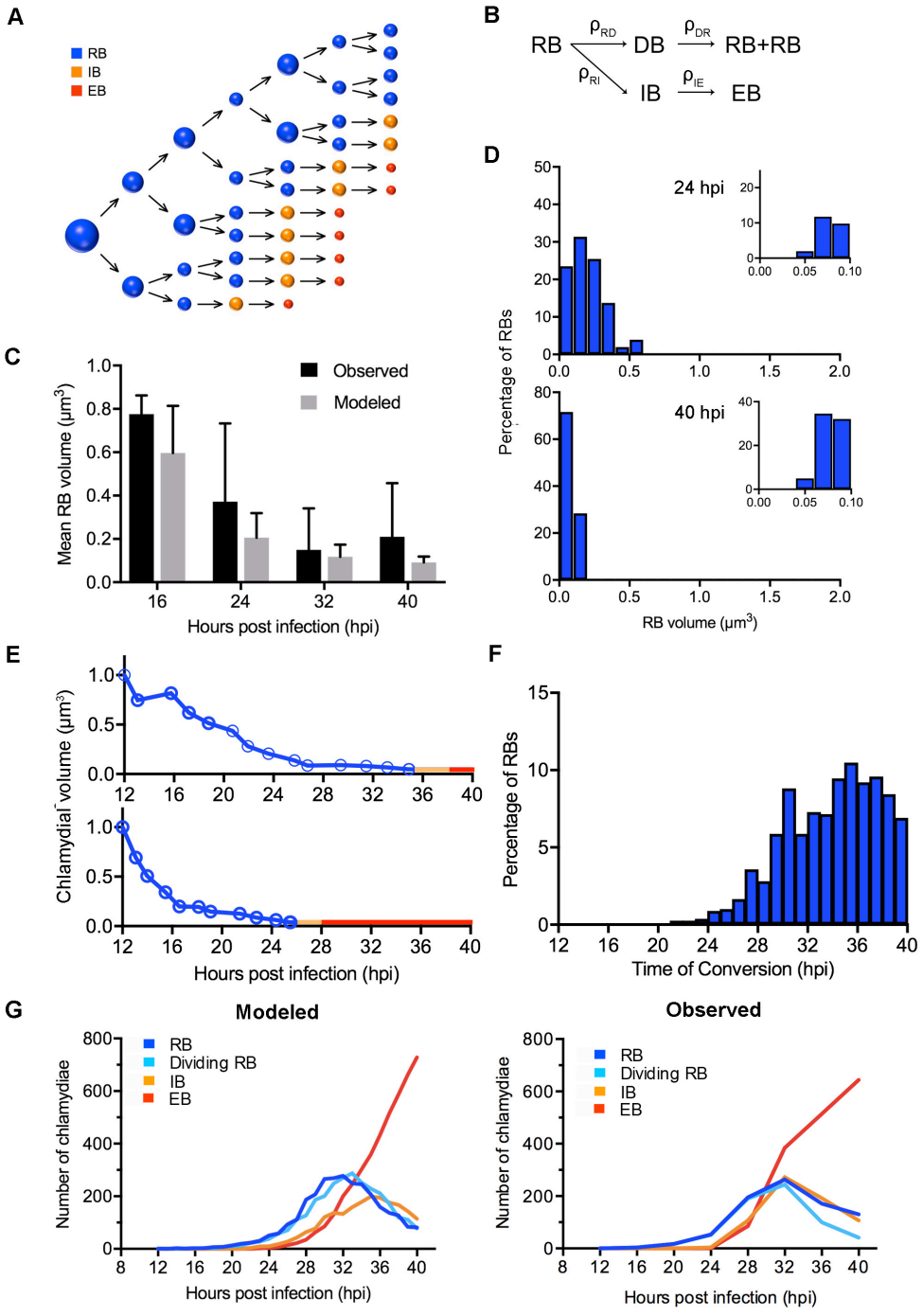

2

Figure 5. Analysis of size-dependent control of RB-to-EB conversion using a stochastic mathematical model.

(A) Proposed model in which the size of an RB determines whether it can convert or continues to replicate. RBs become progressively smaller because they divide, on average, at less than twice their starting size. They can only convert into an EB below a permissive size. These two elements of RB size control ensure that the RB population expands before conversion occurs. The figure demonstrates how weak control of RB size at replication can produce size heterogeneity and lead to asynchronous conversion by varying the number of replication cycles required to reach the conversion size threshold. **(B)** Wiring diagram to show the four different variables in the system and the four possible transformations. Details of the mathematical model provided in Mathematical Analysis in the Supplementary Materials. **(C)** Mean volume of the RB population within an individual inclusion, measured experimentally, or produced by the size control model, at selected time points. Error bars indicate standard deviation. **(D)** Histograms of RB size obtained with the mathematical model for single inclusions at 24 and 40 hpi recapitulate the experimental data in Fig. 3C. **(E)** Two sample time courses from the model illustrating how different RB lineages culminate in different times of RB-to-EB conversion. Each time course consists of successive rounds of RB replication (blue line) followed by conversion to an IB (orange line) and then EB (red line). Each newly produced RB shown by an open circle. **(F)** Histogram showing time of RB-to-EB conversion predicted by the mathematical model for all EBs produced in a single inclusion by 40 hpi. **(G**) Growth curves showing the mean number of each chlamydial form/inclusion. The graph on the left was produced by the stochastic size control model,

while the graph on the right shows growth curves from the 3D EM analysis of *Chlamydia*-infected cells.

Rate	Symbol	Value	Measurement	Notes
Initial RB size	s_0	1 μm^3	direct	Fig. 3A
Initial RB replication time	t_0	12hpi	direct	Fig. 1B
DB daughter cell size variability	σ_u	0.05	direct	Fig. 3B
Mean RB growth rate	μ_R	0.25 h^{-1}	calculated	Fig. 1B, 3B
Mean transition time from RB to DB	ρ_{RD}	0.9 h	calculated	Fig. 1B
Mean transition time from DB to 2RBs	ρ_{DR}	0.9 h	calculated	Fig. 1B
RB growth rate variability	σ_R	0.04 h^{-1}	fit to data	Fig. 5
Mean transition time from small RB to IB	ρ_{RI}	0.1 h	fit to data	Fig. 5
Mean transition time from IB to EB	ρ_{IE}	2.5 h	fit to data	Fig. 5
RB threshold size for conversion	s_{thr}	0.06 μm^3	inferred	Fig. S3A, 3C

Table 1. Parameters for the stochastic mathematical model

Parameter values used in the stochastic mathematical model of cell fate regulation through size control. For each parameter we indicate whether its value was directly measured , calculated, or fit so that the model dynamics (Fig. 5) are consistent with experimental data. For instance, the DB daughter cell size variability σ_u is measured as the standard deviation of the data in Fig. 3B. The RB threshold size for conversion is

inferred from Fig. S3A as the mean IB size at 24 hpi, and also from Fig. 3B as the 10^{th} percentile of RB size in a 24 hpi inclusion.

Methods

Cell culture and *Chlamydia* infections

HeLa cells (ATCC) were grown in Advanced DMEM (4.5 g glucose/L) (Invitrogen) supplemented with 2% fetal bovine serum (FBS) (Hyclone/Thermo Fisher) and 2mM GlutaMAX-I (Invitrogen) in 5% CO_2 at 37°C.

Cell monolayers were infected with *C. trachomatis* serovar L2, strain L2/434/Bu at a multiplicity of infection (MOI) of 3 in sucrose-phosphate-glutamic acid (SPG). Uninfected control experiments were performed as mock infections in SPG alone. Infections were carried out by centrifugation at 700x*g* in a Sorvall Legend Mach 1.6R centrifuge for 1 hour at room temperature. After centrifugation, the inoculum was replaced by fresh cell culture medium and monolayers were incubated at 37°C and 5% CO_2. HeLa Cells and EBs were verified to be free of *Mycoplasma* contamination by PCR [33].

Preparation of culture cells for three-dimensional Electron Microscopy (SBEM)

Chlamydia-infected monolayers were fixed in a solution of 2% paraformaldehyde and 2.5% glutaraldehyde in 0.1 M cacodylate buffer, pH 7.4 for 1 hour. Cells were stained for SBEM as previously reported [16]. Briefly, cells were washed 5X in cold 0.1 M cacodylate buffer then incubated in solution containing 1.5% potassium ferrocyanide and 2% osmium tetroxide supplemented with 2 mM calcium chloride in 0.1 M cacodylate buffer for 30 minutes on ice. After 5X 2 minute washes in doubled distilled water, cells were incubated in 1% thiocarbohydrazide for 10 minutes at room

temperature. Following 5X 2 minute washes in double distilled water at room temperature, cells were placed in 2% osmium tetroxide in double distilled water for 10 minutes at room temperature. Cells were rinsed 5X 2 minutes with double distilled water at room temperature and subsequently incubated in 2% uranyl acetate at 4°C overnight. The next day, cells were washed 5X 2 minutes in double distilled water at room temperature and en bloc Walton's lead aspartate staining was performed for 10 minutes at 60°C. Following 5X 2 minute washes in double distilled water at room temperature, cells were dehydrated using a series of ice-cold graded ethanol solutions and then embedded in Durcupan ACM resin (Electron Microscopy Sciences). The resin was allowed to polymerize in a vacuum oven at 60°C for 48 hours. SBEM imaging was completed using a Gatan automated 3View system (Gatan Inc.) incorporated into a Zeiss Sigma or Merlin Compact Scanning Electron Microscope (Zeiss), and images were recorded at 60 nm cutting intervals. For details on image sizes of micrographs produced from each *Chlamydia*-infected monolayer, see Supplementary Table 1.

3D EM Segmentation and Analysis

Complete three-dimensional reconstructions of *Chlamydia* inclusions were constructed and analyzed using the IMOD image processing software (University of Colorado, Boulder). Inclusion membrane and chlamydial forms were marked on two-dimensional electron micrographs then assembled together to build the 3D models. Numerical and volumetric, analyses were conducted using plug-ins of the IMOD software (3Dmod).

3D models were reconstructed for the inclusion in each of 155 *Chlamydia*-infected cells. 50 inclusions at 12 hpi and 31 inclusions at 16 hpi were analyzed. Because of the labor-intensive nature of segmentation, at least 9 inclusions were analyzed at later time points (4-hour intervals between 20 and 40 hpi) when inclusions were large and contained many chlamydiae. For each of these later time points, representative inclusions were selected by predetermining the volume of > 20 inclusions, sorting them by size into three bins (large, medium and small), and using a random number generator to select at least 3 inclusions per bin for analysis (Supplementary Table 2).

Analysis of RB cell division

A total of 114 dividing RB from two 24 hpi inclusions were analyzed in multiple EM sections of 0.06 µm thickness. For each dividing RB, the plane of constriction [27] was identified so that each of the two nascent daughter cells could be separately segmented. The volumes of the parent dividing RB and each daughter cell were then determined from the 3D reconstruction, and a ratio of each daughter volume/parent volume was calculated.

Mathematical Modeling

A continuous-time, stochastic model of cell-size dynamics was designed using parameters based on experimental data from this study. The transitions from RB to dividing RB (DB), RB to IB, and IB to EB follow the network described in Figure 5B for the population model, with gamma distribution for each transition time. In addition, RB-

to-IB conversion can only occur when size decreases below a specified threshold. In this model, the size of each chlamydia at any given time is defined. The exponential growth rates of RBs and DBs are chosen independently from a normal distribution after each transition. The size of a daughter RB is determined from the size of its mother DB at the time of division, using a binomial partitioning method that introduces randomness in the division. The size of an IB and its successor EB is determined by the size of its RB progenitor before conversion. EB size remains constant after conversion. All modeling was carried out using Matlab; see the Mathematical Analysis in the Supplementary Materials for additional details on this model as well as parameter values. The parameter values of the model are based on experimental data, mostly from direct measurements or computed from experimental values. See Table 1 for the parameters used, as well as their values and the form of derivation. See the Mathematical Analysis in the Supplementary Materials for detailed calculations and additional details of this model.

Statistical Information

For Fig 1B, Fig. 5G, and Fig. S2, all of the four chlamydial forms inside 155 inclusions were identified and counted: 12 hpi (n=50 inclusions), 16 hpi (n=31), 20 hpi (n=22), 24 hpi (n=10), 28 hpi (n=13), 32 hpi (n=10), 36 hpi (n=9), 40 hpi (n=10). Fig. 2 reports the mean volume of these 155 inclusions by time point. Fig. 2C-D, Fig. 3A-B and Fig. S3 present a more time-intensive measurement of mean volume for each of the four chlamydial forms within 140 inclusions: 12hpi (n=50 inclusions), 16 hpi (n=31), 20 hpi (n=22), 24 hpi (n=9), 28 hpi (n=7), 32 hpi (n=8), 36 hpi (n=5), 40 hpi (n=8). For Fig. 4,

all 114 dividing RBs from two inclusions at 24 hpi were analyzed. Fig. 5C is an analysis of mean RB volume for the entire RB population within a single inclusion at 16 hpi (n=8 RBs), 24 hpi (n=40), 32 hpi (n=245), and 40 hpi (n=240). Error bars in all graphs represent standard deviation from the mean.

For Fig. 3A, the progressive decrease in RB size was analyzed with an unpaired t-test and found to be statistically significant between 12 hpi and each of the later time points, e.g. 12 hpi and 16 hpi: $p = 0.00025$, t-value=3.9, df = 45; 12 hpi and 20 hpi: $p < 10^{-7}$, t-value 7.0, df = 39; 12 hpi and 24 hpi: $p < 0.0001$, t-value = 4.6, df = 28.

References

1 Newman, L. *et al.* Global Estimates of the Prevalence and Incidence of Four Curable Sexually Transmitted Infections in 2012 Based on Systematic Review and Global Reporting. *PLoS One* **10**, e0143304, doi:10.1371/journal.pone.0143304 (2015).

2 Batteiger, B. E. & Tan, M. in *Mandell, Douglas, and Bennett's: Principles and Practice of Infectious Diseases* (eds John E. Bennett, Raphael Dolin, & Gerald L. Mandell) 2154-2170 (Elsevier Inc., 2014).

3 CDC. Summary of Notifiable Diseases -- United States, 2014. *MMWR* **63**, 1-152 (2016).

4 Bhosai, S. J., Bailey, R. L., Gaynor, B. D. & Lietman, T. M. Trachoma: an update on prevention, diagnosis, and treatment. *Curr Opin Ophthalmol* **23**, 288-295, doi:10.1097/ICU.0b013e32835438fc (2012).

5 Moulder, J. W. Interaction of chlamydiae and host cells *in vitro*. *Microbiol. Rev.* **55**, 143-190 (1991).

6 Abdelrahman, Y. M. & Belland, R. J. The chlamydial developmental cycle. *FEMS Microbiol Rev* **29**, 949-959 (2005).

7 Tan, I. S. & Ramamurthi, K. S. Spore formation in *Bacillus subtilis*. *Environ Microbiol Rep* **6**, 212-225, doi:10.1111/1758-2229.12130 (2014).

8 Shaw, E. I. *et al.* Three temporal classes of gene expression during the *Chlamydia trachomatis* developmental cycle. *Mol Microbiol* **37**, 913-925 (2000).

9 Belland, R. J. *et al.* Genomic transcriptional profiling of the developmental cycle of *Chlamydia trachomatis*. *Proc Natl Acad Sci U S A* **100**, 8478-8483. (2003).

10 Leighton, S. B. SEM images of block faces, cut by a miniature microtome within the SEM - a technical note. *Scan Electron Microsc*, 73-76 (1981).

11 Denk, W. & Horstmann, H. Serial block-face scanning electron microscopy to reconstruct three-dimensional tissue nanostructure. *PLoS Biol* **2**, e329, doi:10.1371/journal.pbio.0020329 (2004).

12 Holcomb, P. S. *et al.* Synaptic inputs compete during rapid formation of the calyx of Held: a new model system for neural development. *J Neurosci* **33**, 12954-12969, doi:10.1523/JNEUROSCI.1087-13.2013 (2013).

13 Wilke, S. A. *et al.* Deconstructing complexity: serial block-face electron microscopic analysis of the hippocampal mossy fiber synapse. *J Neurosci* **33**, 507-522, doi:10.1523/JNEUROSCI.1600-12.2013 (2013).

14 Helmstaedter, M. Cellular-resolution connectomics: challenges of dense neural circuit reconstruction. *Nat Methods* **10**, 501-507, doi:10.1038/nmeth.2476 (2013).

15 Mikula, S. & Denk, W. High-resolution whole-brain staining for electron microscopic circuit reconstruction. *Nat Methods* **12**, 541-546, doi:10.1038/nmeth.3361 (2015).

16 Ngo, J. T. *et al.* Click-EM for imaging metabolically tagged nonprotein biomolecules. *Nat Chem Biol* **12**, 459-465, doi:10.1038/nchembio.2076 (2016).

17 Ou, H. D. *et al.* A structural basis for the assembly and functions of a viral polymer that inactivates multiple tumor suppressors. *Cell* **151**, 304-319, doi:10.1016/j.cell.2012.08.035 (2012).

18 Puhka, M., Joensuu, M., Vihinen, H., Belevich, I. & Jokitalo, E. Progressive sheet-to-tubule transformation is a general mechanism for endoplasmic reticulum partitioning in dividing mammalian cells. *Mol Biol Cell* **23**, 2424-2432, doi:10.1091/mbc.E10-12-0950 (2012).

19 Shehata, T. E. & Marr, A. G. Effect of temperature on the size of *Escherichia coli* cells. *J Bacteriol* **124**, 857-862 (1975).

20 Taheri-Araghi, S. *et al.* Cell-size control and homeostasis in bacteria. *Curr Biol* **25**, 385-391, doi:10.1016/j.cub.2014.12.009 (2015).

21 Campos, M. *et al.* A constant size extension drives bacterial cell size homeostasis. *Cell* **159**, 1433-1446, doi:10.1016/j.cell.2014.11.022 (2014).

22 Akerlund, T., Nordstrom, K. & Bernander, R. Analysis of cell size and DNA content in exponentially growing and stationary-phase batch cultures of *Escherichia coli*. *J Bacteriol* **177**, 6791-6797 (1995).

23 Kjeldgaard, N. O., Maaloe, O. & Schaechter, M. The transition between different physiological states during balanced growth of *Salmonella typhimurium*. *J Gen Microbiol* **19**, 607-616, doi:10.1099/00221287-19-3-607 (1958).

24 Fantes, P. A. Control of cell size and cycle time in *Schizosaccharomyces pombe*. *J Cell Sci* **24**, 51-67 (1977).

25 Moulder, J. W. 122-124 (The University of Chicago Press, Chicago, 1962).

26 Abdelrahman, Y., Ouellette, S. P., Belland, R. J. & Cox, J. V. Polarized cell division of *Chlamydia trachomatis*. *PLoS Pathog* **12**, e1005822, doi:10.1371/journal.ppat.1005822 (2016).

27 Marr, A. G., Harvey, R. J. & Trentini, W. C. Growth and division of *Escherichia coli*. *J Bacteriol* **91**, 2388-2389 (1966).

28 Motulsky, H. *Intuitive Biostatistics: A Nonmathematical Guide to Statistical Thinking*. (Oxford University Press, 2014).

29 Wilson, D. P., Timms, P., McElwain, D. L. & Bavoil, P. M. Type III secretion, contact-dependent model for the intracellular development of *Chlamydia*. *Bull Math Biol* **68**, 161-178, doi:10.1007/s11538-005-9024-1 (2006).

30 Amodeo, A. A. & Skotheim, J. M. Cell-Size Control. *Cold Spring Harb Perspect Biol* **8**, a019083, doi:10.1101/cshperspect.a019083 (2016).

31 Hanson, B. R. & Tan, M. Transcriptional regulation of the *Chlamydia* heat shock stress response in an intracellular infection. *Mol Microbiol* **97**, 1158-1167, doi:10.1111/mmi.13093 (2015).

32 Johnson, K. A., Tan, M. & Sutterlin, C. Centrosome abnormalities during a *Chlamydia trachomatis* infection are caused by dysregulation of the normal duplication pathway. *Cell Microbiol* **11**, 1064-1073, doi:10.1111/j.1462-5822.2009.01307.x (2009).

33 Ossewaarde, J., de Vries, A., Bestebroer, T. & Angulo, A. Application of a *Mycoplasma* group-specific PCR for monitoring decontamination of *Mycoplasma*-infected *Chlamydia* sp. strains. *Applied and Environmental Microbiology* **62**, 328-331 (1996).